



HAL
open science

Catalog of Ultraviolet Bright Stars: Strategies for UV Occultation Measurements, Planetary Illumination Modeling, and Sky Map Analyses Using Hybrid IUE-Kurucz Spectra

Michael A. Velez, Kurt D. Retherford, Vincent Hue, Joshua A. Kammer, Tracy M. Becker, G. Randall Gladstone, Michael W. Davis, Thomas K. Greathouse, Philippa M. Molyneux, Shawn M. Brooks, et al.

► **To cite this version:**

Michael A. Velez, Kurt D. Retherford, Vincent Hue, Joshua A. Kammer, Tracy M. Becker, et al.. Catalog of Ultraviolet Bright Stars: Strategies for UV Occultation Measurements, Planetary Illumination Modeling, and Sky Map Analyses Using Hybrid IUE-Kurucz Spectra. *The Planetary Science Journal*, 2024, 5, 10.3847/PSJ/ad0e70 . insu-04726511

HAL Id: insu-04726511

<https://insu.hal.science/insu-04726511v1>

Submitted on 10 Oct 2024

HAL is a multi-disciplinary open access archive for the deposit and dissemination of scientific research documents, whether they are published or not. The documents may come from teaching and research institutions in France or abroad, or from public or private research centers.













L'archive ouverte pluridisciplinaire **HAL**, est destinée au dépôt et à la diffusion de documents scientifiques de niveau recherche, publiés ou non, émanant des établissements d'enseignement et de recherche français ou étrangers, des laboratoires publics ou privés.



Distributed under a Creative Commons Attribution 4.0 International License



Catalog of Ultraviolet Bright Stars: Strategies for UV Occultation Measurements, Planetary Illumination Modeling, and Sky Map Analyses Using Hybrid IUE-Kurucz Spectra

Michael A. Velez^{1,2} , Kurt D. Retherford^{2,1} , Vincent Hue³ , Joshua A. Kammer² , Tracy M. Becker^{2,1} ,
G. Randall Gladstone^{2,1} , Michael W. Davis² , Thomas K. Greathouse² , Philippa M. Molyneux² , Shawn M. Brooks⁴ ,
Ujjwal Raut^{2,1} , and Maarten H. Versteeg² 

¹ Department of Physics and Astronomy, University of Texas at San Antonio, 1 UTSA Circle, San Antonio, TX 78249, USA; mvelez@swri.edu

² Southwest Research Institute, 6220 Culebra Road, San Antonio, TX 78238, USA

³ Aix-Marseille Université, CNRS, CNES, Institut Origines, LAM, Marseille, France

⁴ Jet Propulsion Laboratory, California Institute of Technology, 4800 Oak Grove Drive, Pasadena, CA 91109, USA

Received 2023 April 10; revised 2023 November 1; accepted 2023 November 15; published 2024 April 4

Abstract

Ultraviolet spectroscopy is a powerful method to study planetary surface composition through reflectance measurements, atmospheric composition through stellar/solar occultations, transits of other planetary bodies, and direct imaging of airglow and auroral emissions. The next generation of ultraviolet spectrographs (UVS) on board ESA's Jupiter Icy Moons Explorer and NASA's Europa Clipper missions will perform such measurements of Jupiter and its moons in the early 2030s. This work presents a compilation of a detailed UV stellar catalog, named Catalog of Ultraviolet Bright Stars (CUBS), of targets with high intensity in the 50–210 nm wavelength range with applications relevant to planetary spectroscopy. These applications include (1) planning and simulating occultations, including calibration measurements; (2) modeling starlight illumination of dark, nightside planetary surfaces primarily lit by the sky; and (3) studying the origin of diffuse Galactic UV light as mapped by existing data sets from Juno-UVS and others. CUBS includes observations from the International Ultraviolet Explorer (IUE) and additional information from the SIMBAD database. We have constructed model spectra at 0.1 nm resolution for almost 90,000 targets using interpolated Kurucz models (which have a resolution of 1 nm) and, when available, IUE spectra. CUBS also includes robust checks for agreement between the Kurucz models and the IUE data. We also present a tool for which our catalog can be used to identify the best candidates for stellar occultation observations, with applications for any UV instrument. We report on our methods for producing CUBS and discuss plans for its implementation during ongoing and upcoming planetary missions.

Unified Astronomy Thesaurus concepts: [Ultraviolet spectroscopy \(2284\)](#); [Catalogs \(205\)](#); [Europa \(2189\)](#); [Stellar occultation \(2135\)](#)

1. Introduction

Ultraviolet spectroscopy is an important tool for space science. Spectroscopic techniques involving the use of UV-bright stars include, but are not limited to, stellar occultation/appulse observations for atmospheric studies, measurements of dark or shadowed surfaces through starlight illumination, and investigating diffuse UV galactic dust emissions. These applications motivated the creation of a stellar catalog of UV-bright stars in order to provide simpler ways to plan and execute observations that invoke these techniques. The primary motivations for compiling this catalog are NASA's upcoming Europa Clipper mission (Howell & Pappalardo 2020) and ESA's Jupiter Icy Moons Explorer (JUICE) mission (Grasset et al. 2013), which are set to perform transformational science focusing on Jupiter's icy Galilean moons (Europa, Ganymede, and Callisto). The Europa Ultraviolet Spectrograph (Europa-UVS) and JUICE-UVS will conduct a series of observations, including those mentioned above, that require knowledge about the stars in the UV.

UV spectrographs on previous space missions have used these observational techniques, starting with Voyager when its UVS instrument (Broadfoot et al. 1977) first provided an in-depth analysis of Ganymede's exosphere (Broadfoot et al. 1979). Europa-UVS is the latest in a series of spectrographs that will complete significant UV observations throughout the solar system. The first UV instrument in this series, the Alice instrument on ESA's Rosetta mission, was the first UV spectrograph to study a comet (67P/Churyumov–Gerasimenko) at close range (Stern et al. 2007). It used stellar appulse observations to study H₂O and O₂ in the coma of the comet (Keeney et al. 2017). The Alice instrument on NASA's New Horizons mission was the first to closely study Pluto, Charon, and Arrokoth (Stern et al. 2008). During its cruise to Pluto, New Horizons' Alice also observed a stellar occultation by Jupiter's atmosphere that helped to constrain the concentration of compounds such as methane, acetylene, and ethane (Greathouse et al. 2010). At Pluto, New Horizons' Alice observed solar and stellar occultations by Pluto's atmosphere and constrained profiles for nitrogen as well as hydrocarbon compounds (Gladstone et al. 2016; Young et al. 2018; Kammer et al. 2020). The Lyman Alpha Mapping Project (LAMP) instrument on NASA's Lunar Reconnaissance Orbiter (LRO) continues to monitor the Moon's surface and atmosphere (Gladstone et al. 2010). One of its main functions is to analyze



Original content from this work may be used under the terms of the [Creative Commons Attribution 4.0 licence](#). Any further distribution of this work must maintain attribution to the author(s) and the title of the work, journal citation and DOI.

permanently shadowed regions (PSRs) on the surface using starlight illumination rather than sunlight (Gladstone et al. 2012; Byron et al. 2019). Juno-UVS on NASA’s Juno mission studies far-UV (FUV) auroral emissions at Jupiter (Gladstone et al. 2017). Notably, Juno-UVS has obtained a full spectral map of the sky in the UV that is considered in our study (Hue et al. 2019, 2021). Both the upcoming Europa-UVS and JUICE-UVS instruments will also be able to conduct studies of the Jovian system using these techniques. Other important UV instruments include the Cassini Ultraviolet Imaging Spectrograph (UVIS; Esposito et al. 2004), the Spectroscopy for the Investigation of the Characteristics of the Atmosphere of Mars (SPICAM) light UV spectrometer on Mars Express (Bertaux et al. 2000), and the Spectroscopy for the Investigation of the Atmosphere of Venus (SPICAV) UV spectrometer on Venus Express (Bertaux et al. 2007). Cassini UVIS performed stellar and solar occultations by Saturn (Koskinen et al. 2013, 2015) and its rings (Colwell et al. 2010; Becker et al. 2018) as well as by the water vapor plumes of Enceladus (Burger et al. 2007; Hansen et al. 2011). Previous studies also used UVIS stellar occultations during the Cassini Grand Finale to create a 2D global map of densities and temperatures in Saturn’s thermosphere (Brown et al. 2020). SPICAM was able to detect molecular oxygen on Mars using stellar occultation measurements of the planet (Sandel et al. 2015) and further demonstrate how FUV observations are effective for the study of planetary bodies and the galaxy as a whole. Studies using SPICAV data analyzed sulfur dioxide and ozone mixing ratios in the atmosphere of Venus (Evdokimova et al. 2021), showcasing the breadth of atmospheric components detectable by UV occultations.

The Catalog of Ultraviolet Bright Stars (CUBS) initially began as a much smaller endeavor with 1000 stars with available spectra from the International Ultraviolet Explorer (IUE). The catalog was first used to model starlight illumination of the Moon’s surface for LAMP observations (Gladstone et al. 2012; Section 3.2) and was later expanded to 2000 stars by adding other UV-bright stars that could be well represented by Kurucz models (Byron et al. 2019). A separate catalog of Juno-UVS spectra of >500 stellar targets obtained to perform instrument calibrations (Hue et al. 2021) provides a valuable cross-comparison (shown in Section 2) and identified a few targets that had been missing from the original catalog. This paper will discuss the methods used to create this catalog (Section 2), identify three planned direct applications for this catalog (Section 3), and summarize the conclusions of this work, most notably how well the Kurucz models perform when compared to observations (Section 4).

2. Methodology

CUBS currently consists of nearly 90,000 stars of O (~5000), B (~41,000), and A (~42,000) types and exists as a spreadsheet and an IDL save file. The catalog spreadsheet contains specific information about each star (where available) retrieved from the SIMBAD database (Wenger et al. 2000). These data include HD number, common identifier, R.A., decl., spectral type, stellar type, B magnitude, V magnitude, proper motion (both R.A. and decl.), radial velocity, and parallax. All numerical quantities are included with their uncertainties. The IDL save file contains the modeled spectral flux density of each star in CUBS within the wavelength range of 50–210 nm (JUICE-UVS covers a range of 50–204 nm, Davis et al. 2020,

and Europa-UVS similarly covers 55–206 nm, Davis et al. 2022). CUBS is planned to be archived in the NASA Planetary Data System with other Europa-UVS data products as well as a supplement to this paper. Further archival sources, such as MAST, are being considered as well.

The spectra in CUBS were produced using two different methods: Kurucz models alone or a combination of IUE data and Kurucz models. Kurucz models were originally developed in 1979 (Kurucz 1979) and updated in 1992 (Kurucz 1992) with new data and improved spectral resolution, such as a higher number of optical depth layers. The updated Kurucz Atlas contains roughly 7600 stellar atmosphere models with wavelengths ranging from 9 to 160,000 nm at a spectral resolution of 1 nm, which helps ensure the robustness of CUBS spectra for all stellar types. Castelli & Kurucz (2003) updated the stellar model to include interstellar absorptions from 140 to 160 nm, among other improvements. Other interstellar absorptions are also present, including $\text{Ly}\alpha$, but these are not explicitly accounted for in these models. To construct the spectra, we use key parameters for each star, such as its stellar type, to get an applicable effective temperature that can be used as an input to the Kurucz model. Other inputs include the surface gravity ($\log g$), which our model defaults to the highest possible value ($\log g = 5$) for a given estimated effective temperature, and metallicity ($\log z$), which is set to $\log z = 0$ to represent the average of the possible parameter space (-5 to 5) of the star. For stars that have $\log g$ and $\log z$ values in the SIMBAD database, we use the median reported values in CUBS. To estimate the effect of varying the $\log g$ and $\log z$ values in the Kurucz models of stars that had reported values in the SIMBAD database versus the default values used, we analyzed the relative differences between the spectra. Across the entire bandpass, the average relative differences measured over the 1950 stars with reported $\log g$ and $\log z$ values vary by ~15%. The B and V magnitudes for each star are then applied to redden the spectra as they would be observed from the solar system. We then interpolate the Kurucz data to obtain our desired 0.1 nm resolution.

These Kurucz models are supplemented by observational data from the IUE where available. The IUE was launched in 1978 to observe UV-bright stars, specifically using two spectrographs with a range of 115–200 and 185–330 nm with spectral resolutions ranging from 0.02 to 0.6 nm (Boggess et al. 1978). Throughout the entire duration of the mission, IUE observed over 100,000 targets, of which around 1800 have spectra that were appropriate to use for Juno-UVS calibrations (Hue et al. 2021) and are also used in our catalog. The IUE spectra we use in CUBS range from 116 to 196 nm, which sometimes includes data from one or both IUE spectrographs. We extended these spectra out to the full range of CUBS by normalizing the Kurucz spectra to the IUE data via interpolation and appending them to the short-end, extreme-UV (EUV; 50–116 nm) and long-end, FUV (196–210 nm) wavelength regions for UVS. For the purposes of modeling the estimated signal measured by a specific UV instrument, the stellar flux can be converted to an instrument response using its effective area curve, i.e., the effective area of the telescope mirror after accounting for the throughput losses. Figure 1 shows an example of both a flux spectrum and an instrument count spectrum for Europa-UVS.

Comparing model-predicted stellar spectra with UV observations from space telescopes increases the level of confidence

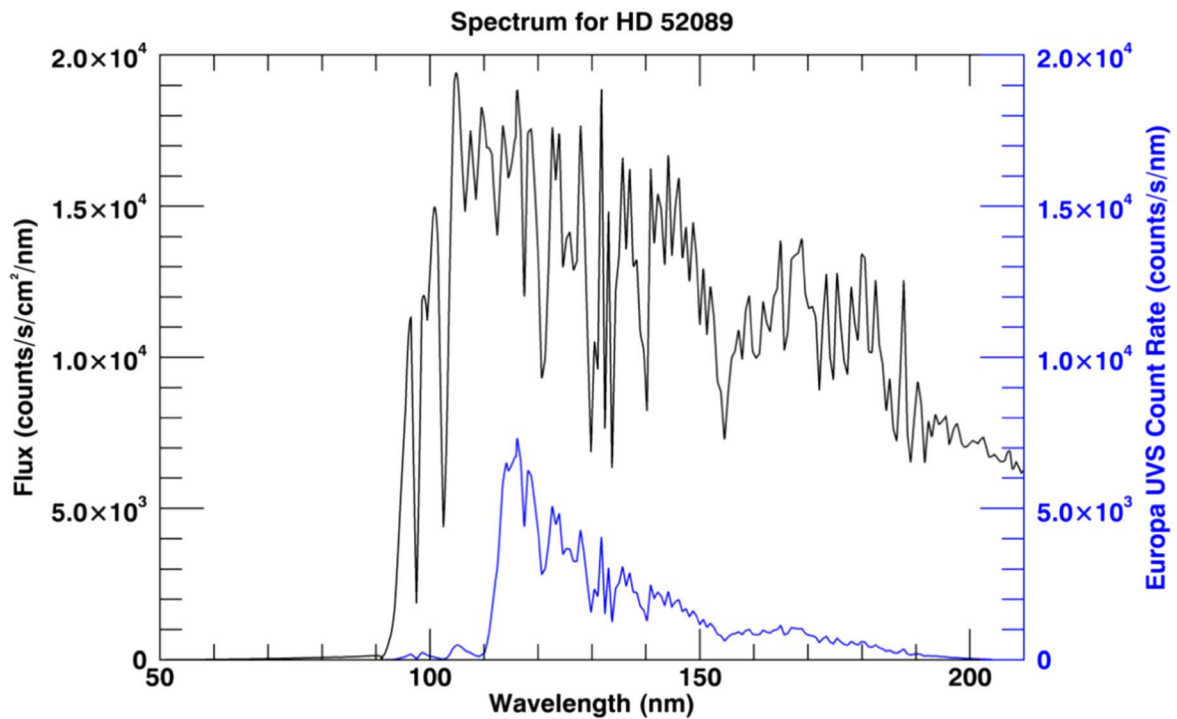


Figure 1. Example spectra from CUBS with both the flux of the star (black) and the estimated count rate (blue) as expected to be viewed by Europa-UVS. IUE data are used between 116 and 196 nm, and a Kurucz model is used between 50–116 and 196–210 nm.

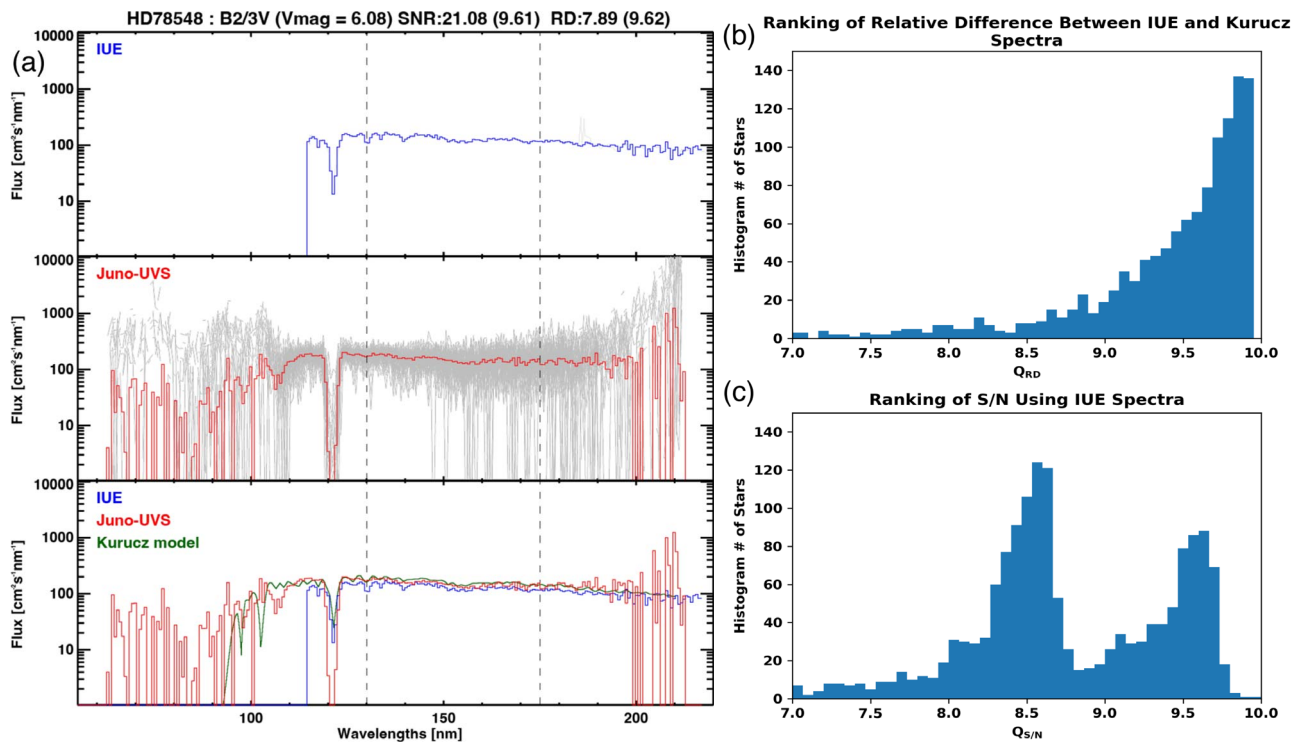


Figure 2. (a) Comparison of IUE (blue), Juno-UVS (red), and Kurucz (green) spectra for HD 78548. The gray lines are the total data for both IUE and Juno-UVS with the colored lines being the averages. The dashed lines are the cutoff of 130–175 nm used for the confidence factors. It should be noted that Juno-UVS is experiencing a localized gain loss at Ly α (gain sag), an effect previously documented (Hue et al. 2019). This is one of many examples showing how effective the Kurucz models can be to construct CUBS spectra. (b) Histogram of quality ranking [0, 10] for all IUE stars in CUBS based on the relative difference (RD) between IUE and Kurucz spectra between 130 and 175 nm. (c) Histogram of quality ranking [0, 10] for all IUE stars in CUBS based on the S/N of IUE spectra between 130 and 175 nm.

in these models, as demonstrated in Figure 2. As the brightnesses of the majority of targets in CUBS exceed the bright object limits of Hubble Space Telescope UV instruments, we rely on the Juno-UVS data set for our quality check.

The Juno-UVS data’s spectrograph resolution of 1.3 nm was Nyquist sampled with spectral bins of 0.65 nm. As targets are used in the future, the catalog is expected to be updated as needed in any cases where the estimated spectra are not met

within 10% accuracy. Figure 2(a) shows an IUE spectrum, a Juno-UVS spectrum, and a comparison plot with Kurucz spectra. To quantify the confidence of the Kurucz model spectra's ability to match the IUE observed spectra, we created the following quality metric:

$$RD = \left| \frac{F_{IUE} - F_{Kurucz}}{F_{IUE} + F_{Kurucz}} \right|, \quad (1)$$

$$Q_{RD} = 10 + \ln \left(\frac{RD_{Max} - RD}{RD_{Max}} \right). \quad (2)$$

RD refers to the relative difference, and RD_{Max} is the maximum relative difference in the data set (found to be 24, when comparing the IUE and Juno-UVS spectra). Q_{RD} is the ranked quality from 0 to 10 that provides a simplified metric for determining whether the spectra are well matched between the IUE catalog and the Kurucz models, with a histogram shown in Figure 2(b). F_{IUE} and F_{Kurucz} are the total fluxes within the wavelength range of 130–175 nm of the IUE and Kurucz data, respectively. This range was chosen because it corresponds to a molecular oxygen (O_2) absorption feature, an important atmospheric constituent to detect on icy moons such as Europa. For example, it has also been detected in previous stellar occultations by Mars by SPICAM (Sandel et al. 2015) and by the stellar appulse of comet 67P/Churyumov–Gerasimenko (Keeney et al. 2017). Currently, those stars that have a low Q_{RD} are planned to be examined on a case-by-case basis to determine the reason for the discrepancy between the model and the observed spectra.

To ensure the confidence and quality of the IUE spectra, we created a separate quality ranking metric for the signal-to-noise ratio (S/N), hereafter also $\eta_{S/N}$, of the IUE spectra once again within the desired wavelength range of 130–175 nm:

$$Q_{S/N} = 10 + \ln \left(\frac{\eta_{S/N}}{(\eta_{S/N})_{Max}} \right). \quad (3)$$

Figure 2(c) shows a histogram of the S/N quality ranking for the considered stellar distribution. To get the arbitrary quality ranking from 0 (worst) to 10 (best) for this additional $Q_{S/N}$ metric, we used Equation (3), where the $(\eta_{S/N})_{Max}$ was found to be 31. Note that the bimodal distribution seen in Figure 2(c) is caused by the two dispersion modes available to IUE. These quality assessments are available for each of the 1800 IUE stellar targets used in CUBS and unavailable for the remaining Kurucz-model-only targets. These assessments are also currently only focused on the 130–175 nm wavelength range and thus may not be as robust for the shorter or longer wavelengths.

3. Planned Applications

3.1. Stellar Occultations

One primary planned use of CUBS is to model stellar occultation observations that will be observed by Europa-UVS and JUICE-UVS, which can provide a wealth of information relevant for atmospheric studies. A stellar occultation occurs when an observed background star passes behind a target of interest. If the star passes sufficiently close to but never behind the solid body of the target, the observation is referred to as a stellar appulse and can still provide constraints on the

composition of the atmosphere above the limb. As the starlight passes through the atmosphere of the target, its observed spectrum will display absorption signatures at the relevant wavelengths of the components present in the atmosphere. The depth and width of the absorption feature ultimately indicate the abundance of that specific compound, which can be monitored until the star is completely obstructed by the solid surface. Using the absorption cross sections for each component, these data can be analyzed to provide direct information about the composition of the atmosphere as a function of altitude above the body's surface. In addition, occultation observations can be used to provide astrometric information on the topographic shape of a target based on the time of complete signal obscuration, as is planned to be done on Europa by Europa-UVS (Abrahams et al. 2021). This process has been successfully implemented for constraining the sizes of asteroids in our solar system, such as the Trojan asteroids Patroclus and Menoetius (Buie et al. 2015).

These occultation events are time-critical and need to be planned in advance. To maximize their impact, a quality factor can be established when ranking the possible choices of events to schedule. For a spacecraft such as Europa Clipper that will be orbiting Jupiter and performing close flybys of Europa, and considering that CUBS has almost 90,000 targets, there are many possible candidates for occultation measurements throughout the course of the mission. Establishing a semi-quantitative quality factor allows for an efficient way of determining which stars will be the best targets during the course of the mission. Of nearly 90,000 potential targets, we expect the top ~25% of stars to be of sufficient quality to have the most use in practice. Any subsequent criteria to filter potential target stars would be dependent on the objectives and specifics of the particular mission.

To create the quality factor, we start by using the measured effective area for the instrument in question to convert CUBS stellar flux spectra to the instrument count rate spectra. In this work, we consider the effective area for Europa-UVS and JUICE-UVS. Next, we isolate an “on-band” region that corresponds to O_2 absorption ranging from 130 to 175 nm. While H_2O and several other expected species have detectable UV absorption features (Figure 3; see also Table 1), O_2 is expected to be the easiest species to measure globally in Europa's atmosphere due to its relatively large abundance (Roth et al. 2016) and hence is the best for setting a minimum criterion to determine whether an observation is useful or not. Additional observations planned for astrometric characterizations of the solid surface shape will be defined with a looser minimum criterion for its usefulness based on a complete attenuation of signal at all wavelengths. For the O_2 on-band range, the count rate (R_{On}) and expected total counts (C_{On}) over a defined integration period during the occultation can be determined for Europa-UVS using the following equations:

$$r = \frac{\text{On-band occultation Count Rate}}{\text{On-band baseline Count Rate}} = \frac{R_{On}}{R_{On_0}}, \quad (4)$$

$$R_{On} = R_{On_0} * r, \quad (5)$$

$$t_{int} = \frac{H}{v_{los}}, \quad (6)$$

$$C_{On} = R_{On} * t_{int}. \quad (7)$$

R_{On_0} is the unocculted on-band rate presented in the catalog and, after rearranging Equations (4) and (5), can be multiplied

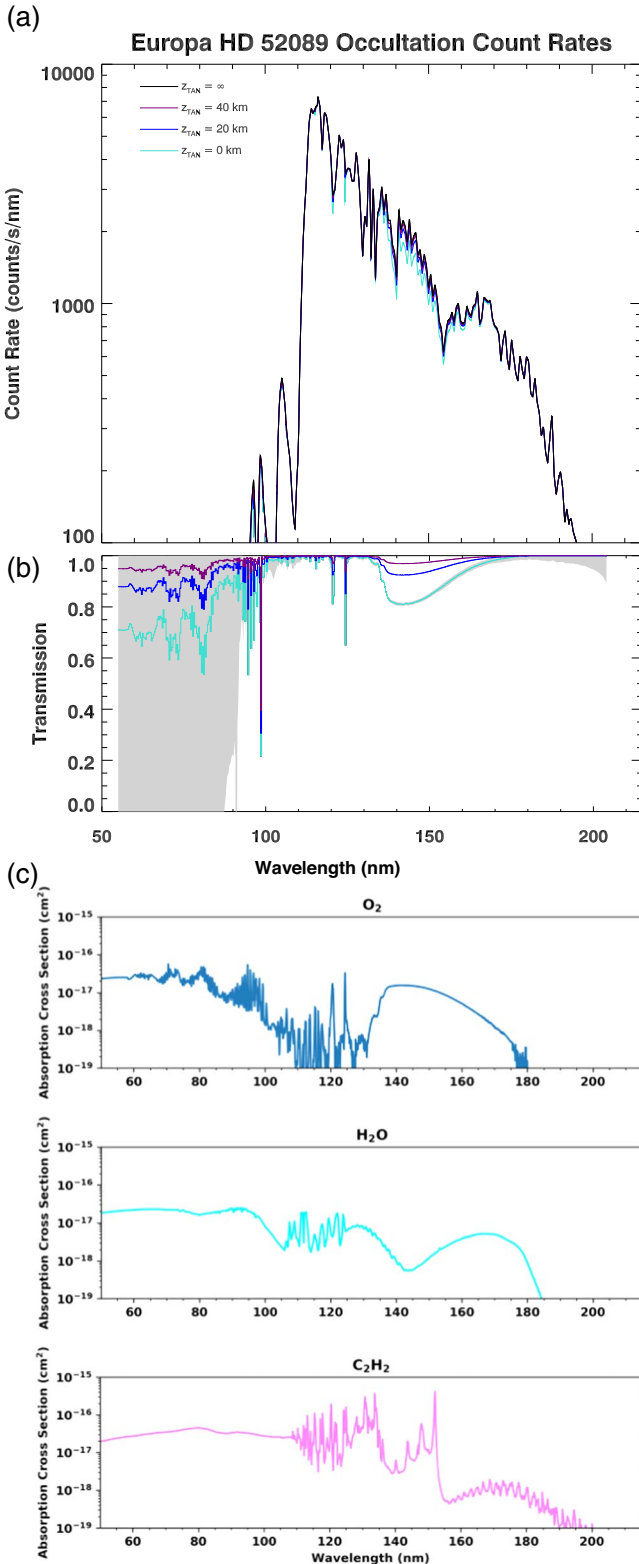


Figure 3. Example (a) stellar occultation spectra and (b) transmission spectra from star HD 52089 showing how the stellar signal decreases in intensity at specific wavelengths related to the composition of a model for Europa’s atmosphere as the star gets closer to the surface (altitude $Z_{TAN} = 0$ km) from the reference frame of the observing spacecraft. The gray region represents the 1σ uncertainty for the transmission spectra. (c) Absorption cross sections for key species in Europa’s atmosphere (O_2 , H_2O , and C_2H_2) used in the present model (references shown in Table 1).

Table 1

References for Relevant Species Cross Sections with Corresponding Temperatures

Species	Temperature (K)	References
O_2	298	Brion et al. (1979)
	298	Matsunaga & Watanabe (1967)
	303.7	Lu et al. (2010)
	298	Ogawa & Ogawa (1975)
	298	Watanabe & Marmo (1956)
H_2O	298	Ogawa (1971)
	298	Chan et al. (1993)
H_2O	298	Mota et al. (2005)
	298	Nakayama & Watanabe (1964)
C_2H_2	298	Cooper et al. (1995)
	295	Chen et al. (1991)

with the transmission of the starlight through the atmosphere (r) to obtain R_{On} . Equation (6) shows how to calculate the integration time of the occultation (t_{int}), which is the time while the star’s light is being occulted by the target’s atmosphere within its scale height (H). The scale height of an atmosphere is defined as the distance over which the pressure decreases by an exponential factor (de Pater & Lissauer 2015). In this paper, we use the scale height as a constant length scale over which we apply the absorption feature in the on-band. For Europa, we set this length to 50 km for the general atmosphere and 30 km for a plume region. These are simply rough estimates that would be further informed by any mission results and detailed forward modeling. The velocity term v_{los} is related to the angular line-of-sight velocity of the star projected to Europa’s sky plane. Once R_{On} and t_{int} are known, we can find the total expected counts over the on-band range (C_{On}) using Equation (7).

We can also calculate C_{On_0} , which represents the total counts in the on-band wavelength region of the unocculted star to serve as a baseline for the lightcurve (i.e., the measured signal as a function of time):

$$C_{On_0} = R_{On_0} * t_0. \quad (8)$$

The baseline time (t_0) to get these initial counts is meant to be time spent above 400 km at Europa. Nominally, the goal is to get 10 minutes of baseline time, but any time period that achieves an $\eta_{S/N} > 3$ for the lightcurve as a whole is sufficient. Recall that $\eta_{S/N} > 3$ is our minimum for selecting potential events for further prioritization in the actual scheduling of observing sequences. Once the counts are determined, an expected absorption in signal can be determined based on a canonical example modeled atmosphere as explained later in this section. This absorption in the signal is calculated using

$$a = 1 - r, \quad (9)$$

where a refers to the aforementioned absorption feature in the lightcurve during the occultation. The absorption then goes through a propagation of error to determine its uncertainty:

$$\sigma_{C_{On}} = \sqrt{C_{On}}, \quad (10)$$

$$\begin{aligned}\sigma_a &= \sigma_r = r \sqrt{\left(\frac{\sigma_{C_{On}}}{C_{On}}\right)^2 + \left(\frac{\sigma_{C_{On0}}}{C_{On0}}\right)^2} \\ &= r \sqrt{\left(\frac{\sqrt{C_{On}}}{C_{On}}\right)^2 + \left(\frac{\sqrt{C_{On0}}}{C_{On0}}\right)^2} = r \sqrt{\frac{1}{C_{On}} + \frac{1}{C_{On0}}}. \quad (11)\end{aligned}$$

Equation (10) states that the uncertainty of a signal can be represented by the square root of the counts. The uncertainty found in Equation (11) (σ_a) is then used to calculate the absorption $\eta_{S/N}$ given by

$$\eta_{S/N_a} = \frac{a}{\sigma_a} = \frac{a}{r \sqrt{(1/C_{On}) + (1/C_{On,0})}}. \quad (12)$$

In total, we have three different regimes for absorption criteria that depend on the target science objective. The first is the case of a general atmosphere, where we set the O₂ absorption feature to be a 10% drop in the count rate and we use 50 km for the scale length. The second case is a plume-dominated region, where the absorption is set to be 50% to represent that an atmospheric enhancement would appear above the nominal signal, and the scale length is 30 km to represent the altitude range where the plume's ejecta will likely dominate. The last case is full obstruction behind Europa, where there would be no transmission of light; this will be used for astrometry. In this case, the scale length is set to 100 m, and the count rate is measured across the entire wavelength range, not just the on-band, because it is not composition-dependent. The absorption values of 10%, 50%, and 100% for exosphere, plume, and limb/astrometric target types and target-dependent scale lengths are established ad hoc in a relative sense to avoid the need for complex forward modeling of atmospheres within the planning process to select the best events. Figure 3 shows an example of absorption through Europa's atmosphere that uses a more sophisticated model than needed for this initial quality factor that can be employed once a narrowed list of candidates has been established using our quality factor.

Other signals in the spectra include Europa disk reflectance as well as airglow emissions and radiation-induced detector noise, which is straightforward to subtract in our signal but adds additional uncertainties. For stars brighter than Europa's disk reflectance, this noise correction will be largely ignorable, as shown by

$$\sigma_{C_{On}} = \sqrt{\frac{1}{C_{On}} + \text{Noise}^2}. \quad (13)$$

η_{S/N_a} gives a quality factor that helps rank the subjective quality of the stellar occultation as "very good," "good," "OK," or "bad." These rankings correspond to $\eta_{S/N}$'s of >100, 10–100, 3–10, and <3, respectively. The "OK" ranking corresponds to meeting a minimum baseline $\eta_{S/N}$ of 3 for further consideration in event observation planning, with the expectation that higher-quality ranked events will be primarily chosen for scheduling when available. Once the categories are established using the semiquantitative quality factor, additional subjective criteria can also be employed to move an occultation up or down in ranking. These criteria are dependent on the objectives and specifics of the particular mission. For example,

Europa-UVS has the criteria listed below, which are subject to change as the mission progresses.

1. Fills global location and time coverage needs.
2. Passes through candidate plume locations.
3. Previously observed with Europa-UVS.
4. Has IUE or other known spectra, not only models.
5. Low flux variability and/or high accuracy of parameters such as astrometry.
6. Emphasizes EUV (<115 nm) capability and sensitivity to additional species.
7. Pair of events, two cords at once (lines connecting ingress and egress for astrometric calculations), or proximity to another UV-bright star.
8. Times when background radiation levels near the spacecraft are low.
9. Follows the Clipper trajectory line of sight for best in situ (MASPEX + SUDA) comparisons.
10. Lines up with radar (REASON) ground track for best astrometry correlation.
11. Coincides with images (EIS) of high phase limb plume search locations.
12. Relatively less auroral brightness, impacting cases with borderline S/N.
13. Near-simultaneity with JUICE encounters.
14. Near-simultaneity with JUICE-UVS occultation observations.

This process is currently being utilized by the Europa-UVS planning team and can be replicated for any other UV mission/instrument (including plans for JUICE-UVS) given knowledge of the instrument effective area and defined set of spacecraft trajectories during the mission lifetime. With other targets, the parameters of the atmospheric scale length and on-band wavelength band used in the quality algorithm will need to be adapted. Table 2 shows several targets with example values that can be plugged into the quality factor equations in lieu of the Europa numbers. As with our numbers for Europa Clipper observation planning, such rough estimates for scale lengths would be further informed by any mission results and detailed forward modeling but are not needed for our present focus of event observation planning.

3.2. Starlight Illumination Modeling

Another intended use of CUBS involves starlight illumination modeling, which allows for surface reflectance studies of various airless solar system bodies. This activity is performed by using a UV spectrograph to observe a target's nightside surface when there is no background light from the Sun. As a result, the only light shining on the surface is that from UV-bright stars and other background sources (background sky, Jupiter shine, satellite shine), and so any reflectance observed by the spectrograph is a result of all of these diffuse background illumination sources. The reflectance can then be analyzed at specific wavelengths to characterize the surface composition and microphysical structure (e.g., compaction/porosity), as for dayside sunlit imaging.

This approach was demonstrated using an earlier version of the catalog at the Moon to study its PSRs and on the lunar nightside using the LAMP instrument on NASA's LRO (Gladstone et al. 2012; Byron et al. 2019). Byron et al. (2019) expanded the initial IUE-based catalog using Kurucz models and added the Large and Small Magellanic Clouds as UV illumination sources based on

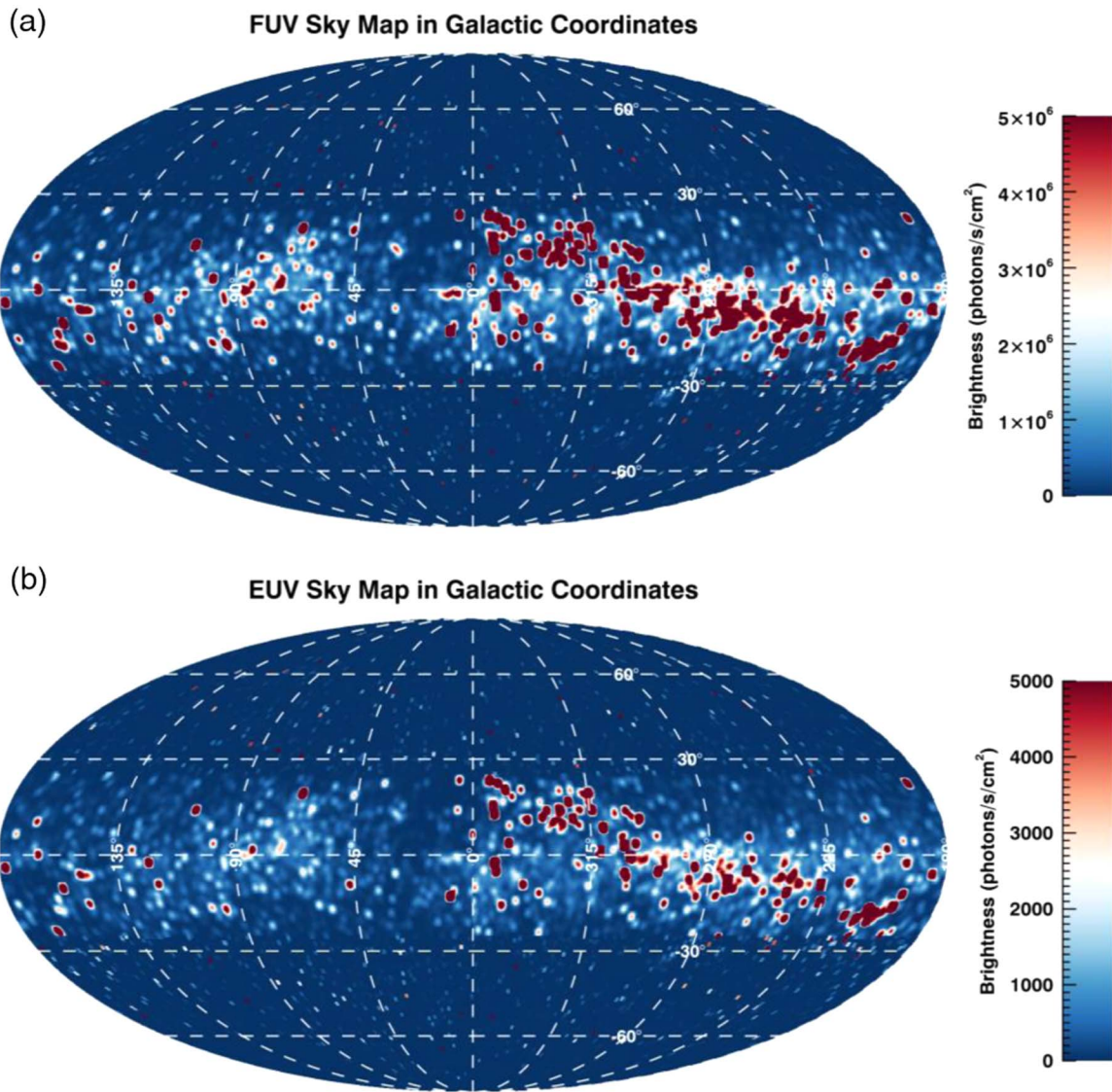


Figure 4. (a) FUV sky map created using CUBS integrated from 115 to 210 nm. (b) EUV sky map integrated from 50 to 115 nm.

Table 2
Parameters for Occultation Bodies of Interest

Target	Element/Compound of Interest	On-band (nm)	Absorption Percentage	Scale Length ^a (km)	References
Europa	O ₂	130–175	10%	50	...
Europa (plume)	H ₂ O	130–175	50%	30	...
Ganymede	O ₂	130–175	10%	100	(1)
Callisto	O ₂	130–175	10%	30	(2)
Io	SO ₂ or O ₂	120–135 (SO ₂)	10%	100	(3)
		130–175 (O ₂)	10%		
Jupiter	H ₂ or CH ₄	100–112 (H ₂)	10%	24	(4)
		111–140 (CH ₄)	100%		
Titan	N ₂ or CH ₄	65–100 (N ₂)	10%	15–50	(5)
		111–140 (CH ₄)	10%		
Triton	N ₂ or CH ₄	65–100 (N ₂)	10%	9	(6)
		111–140 (CH ₄)	10%		
Pluto	N ₂ or CH ₄	65–100 (N ₂)	10%	115–150	(7)
		111–140 (CH ₄)	10%		
Mars	CO ₂	120–180	10%	95–120	(8)
Venus	CO ₂	120–180	10%	4	(9)

Note.

^a Scale lengths are the distance above the exobase or $\tau = 1$ optical depth depending on the body.

References. (1) Roth et al. (2021), (2) Cunningham et al. (2015), (3) Roth et al. (2011), (4) Greathouse et al. (2010), (5) Hörst (2017), (6) Strobel et al. (1990), (7) Young et al. (2018), (8) Sandel et al. (2015), (9) Piccialli et al. (2015).

Juno-UVS observations of these extended sources (Hue et al. 2019). They used LRO LAMP observations during nighttime to create brightness maps and then divided by the incident stellar illumination predicted by the catalog to create an FUV albedo map of the Amundsen crater on the Moon. Their results from these observations were important in determining that the albedo of the PSR inside the crater is lower than the surrounding regions, allowing them to estimate the porosities of the regolith. The catalog in its current, further-expanded state allows for a more accurate representation of the background stars contributing to the illumination of nightside surfaces. We plan to implement CUBS when modeling the stellar, interplanetary Ly α and helium skyglow, and Jupiter-shine illumination of the nightside surfaces of Europa, Ganymede, and Callisto as viewed by Europa-UVS and JUICE-UVS.

3.3. Galactic UV Sky Map

Another intended use of CUBS involves studying diffuse Galactic UV dust emissions. By plotting each star by location using their R.A. and decl. along with their fluxes, we can make a sky map in the UV. We specifically integrated first from 115 to 210 nm to cover the FUV range and next from 50 to 115 nm to cover the EUV range (Figure 4). After applying boxcar smoothing of width 2 along the Galactic plane, we directly compared the maps derived from the spectral models to maps generated by Juno-UVS (Gladstone et al. 2017) and other UV instruments. Through comparisons between observations and our modeled sky, we find that CUBS serves as a reliable representation of the stars present in the Galaxy and their fluxes. However, there is an apparent glow, especially along the Galactic plane, that is observed by Juno-UVS but cannot be completely modeled with just the included stars, indicating that additional UV sources (for example, dust-scattered light from background UV stars) are present. This unmodeled glow requires further study, and CUBS will be useful for separating the dust glow from the stellar components. A similar photometric simulation based on IUE catalog sources has been applied to the Galaxy Evolution Explorer data set for similarly isolating the nonstellar sources (Beitia-Antero & Gómez de Castro 2016).

4. Conclusions

A robust UV stellar catalog, such as the one presented here, can serve as an invaluable resource for performing UV spectroscopic studies that utilize UV-bright stars. CUBS was created using a combination of Kurucz models and IUE spectra, where available. For those stars with available IUE spectra, we compared the Kurucz and the IUE spectra to assess the efficacy of the Kurucz models. We also compared these spectra to those available from Juno-UVS calibration observations to further provide a confidence test for the Kurucz models. We found that there is a strong agreement between them, which demonstrates that the models are sufficiently reliable for the purposes of observation planning. This paper also discussed three possible applications of CUBS:






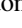






1. planning and simulating stellar occultations;
2. modeling the illumination of dark, nightside planetary surfaces primarily lit by the background sky; and
3. investigating the origin of diffuse galactic UV light as hinted by previous UV data sets.

Stellar occultations are a key tool for studying atmospheric compositions and structure throughout the solar system. Starlight illumination modeling is important for analyzing surface composition in otherwise dark regions on planetary surfaces. Future UV sky map investigations are needed to understand the full extent of the diffuse components that contribute to the galaxy's glow. Several planned uses were described for supporting the upcoming Europa Clipper and JUICE mission UV investigations.

Acknowledgments

This work expands upon an SPIE Proceedings paper submitted for the 2022 SPIE Astronomical Telescopes and Instrumentation Conference (Velez et al. 2022). This work was supported by NASA through the Europa Clipper Project. The research was carried out in part at the Jet Propulsion Laboratory, California Institute of Technology, under a contract with the National Aeronautics and Space Administration (80NM0018D0004).

ORCID iDs

Michael A. Velez  <https://orcid.org/0000-0001-5835-2250>
 Kurt D. Retherford  <https://orcid.org/0000-0001-9470-150X>
 Vincent Hue  <https://orcid.org/0000-0001-9275-0156>
 Joshua A. Kammer  <https://orcid.org/0000-0002-3441-3757>
 Tracy M. Becker  <https://orcid.org/0000-0002-1559-5954>
 G. Randall Gladstone  <https://orcid.org/0000-0003-0060-072X>
 Michael W. Davis  <https://orcid.org/0000-0003-4338-1635>
 Thomas K. Greathouse  <https://orcid.org/0000-0001-6613-5731>
 Philippa M. Molyneux  <https://orcid.org/0000-0002-4725-4775>
 Shawn M. Brooks  <https://orcid.org/0000-0001-8622-0829>
 Ujjwal Raut  <https://orcid.org/0000-0002-6036-1575>
 Maarten H. Versteeg  <https://orcid.org/0000-0002-2503-9492>

References

- Abrahams, J. N. H., Nimmo, F., Becker, T. M., et al. 2021, *E&SS*, 8, 7
 Becker, T. M., Colwell, J. E., Esposito, L. W., Attree, N. O., & Murray, C. D. 2018, *Icar*, 306, 171
 Beitia-Antero, L., & Gómez de Castro, A. I. 2016, *A&A*, 596, A49
 Bertaux, J.-L., Fonteyn, D., Korablev, O., et al. 2000, *P&SS*, 48, 1303
 Bertaux, J.-L., Nevejans, D., Korablev, O., et al. 2007, *P&SS*, 55, 1673
 Boggess, A., Carr, F. A., Evans, D. C., et al. 1978, *Natur*, 275, 372
 Brion, C. E., Tan, K. H., van der Wiel, M., & van der Leeuw, P. E. 1979, *JESRP*, 17, 101
 Broadfoot, A. L., Belton, M. J. S., Takacs, P. Z., et al. 1979, *Sci*, 204, 979
 Broadfoot, A. L., Sandel, B. R., Shemansky, D. E., et al. 1977, *SSRv*, 21, 183
 Brown, Z., Koskinen, T., Müller-Wodarg, I., et al. 2020, *NatAs*, 4, 872
 Buie, M. W., Olkin, C. B., Merline, W. J., et al. 2015, *AJ*, 149, 113
 Burger, M. H., Sittler, E. C., Johnson, R. E., et al. 2007, *JGRA*, 112, A06219
 Byron, B. D., Retherford, K. D., Greathouse, T. K., et al. 2019, *JGRE*, 124, 823
 Castelli, F., & Kurucz, R. L. 2003, in IAU Symp. Proc. 210, Modelling of Stellar Atmospheres, Poster Contributions, ed. N. Piskunov, W. W. Weiss, & D. F. Gray (San Francisco, CA: ASP), A20
 Chan, W. F., Cooper, G., & Brion, C. E. 1993, *CP*, 178, 387
 Chen, F., Judge, D. L., Wu, C. Y. R., et al. 1991, *JGR*, 96, 17519
 Colwell, J. E., Esposito, L. W., Jerousek, R. G., et al. 2010, *AJ*, 140, 1569
 Cooper, G., Olney, T. N., & Brion, C. E. 1995, *CP*, 194, 175
 Cunningham, N. J., Spencer, J. R., Feldman, P. D., et al. 2015, *Icar*, 254, 178
 Davis, M. W., Gladstone, G. R., Giles, R. S., et al. 2020, *Proc. SPIE*, 11444, 4
 Davis, M. W., Retherford, K. D., Molyneux, P. M., et al. 2022, *Proc. SPIE*, 12181, 38
 de Pater, I., & Lissauer, J. J. 2015, Planetary Sciences (2nd ed.; Cambridge: Cambridge Univ. Press)

- Esposito, L. W., Barth, C. A., Colwell, J. E., et al. 2004, *SSRv*, **115**, 299
- Evdokimova, D., Belyaev, D., Montmessin, F., et al. 2021, *JGRE*, **126**, e2020JE006625
- Gladstone, G. R., Persyn, S. C., Eterno, J. S., et al. 2017, *SSRv*, **213**, 447
- Gladstone, G. R., Retherford, K. D., Egan, A. F., et al. 2012, *JGRE*, **117**, E00H04
- Gladstone, G. R., Stern, S. A., Ennico, K., et al. 2016, *Sci*, **351**, 1280
- Gladstone, G. R., Stern, S. A., Retherford, K. D., et al. 2010, *SSRv*, **150**, 161
- Greathouse, T. K., Gladstone, G. R., Moses, J. I., et al. 2010, *Icar*, **208**, 293
- Grasset, O., Dougherty, M. K., Coustenis, A., et al. 2013, *P&SS*, **78**, 1
- Hansen, C. J., Shemansky, D. E., Esposito, L. W., et al. 2011, *GeoRL*, **38**, 11
- Hörst, S. M. 2017, *JGRE*, **122**, 432
- Howell, S. M., & Pappalardo, R. T. 2020, *NatCo*, **11**, 1311
- Hue, V., Giles, R. S., Gladstone, G. R., et al. 2021, *JATIS*, **7**, 4
- Hue, V., Gladstone, G. R., Greathouse, T. K., et al. 2019, *AJ*, **157**, 90
- Kammer, J. A., Gladstone, G. R., Young, L. A., et al. 2020, *AJ*, **159**, 26
- Keeney, B. A., Stern, S. A., A'Hearn, M. F., et al. 2017, *MNRAS*, **469**, S158
- Koskinen, T. T., Sandel, B. R., Yelle, R. V., et al. 2013, *Icar*, **226**, 1318
- Koskinen, T. T., Sandel, B. R., Yelle, R. V., et al. 2015, *Icar*, **260**, 174
- Kurucz, R. L. 1979, *ApJS*, **40**, 1
- Kurucz, R. L. 1992, in IAU Symp. Proc 149, The Stellar Populations of Galaxies, ed. B. Barbuy & A. Renzini (Dordrecht: Kluwer), 225
- Lu, H.-C., Chen, H.-K., Chen, H.-F., Cheng, B.-M., & Ogilvie, J. F. 2010, *A&A*, **520**, A19
- Matsunaga, F. M., & Watanabe, K. 1967, *Science of Light*, **16**, 31
- Mota, R., Parafita, R., Giuliani, A., et al. 2005, *CPL*, **416**, 152
- Nakayama, T., & Watanabe, K. 1964, *JChPh*, **40**, 558
- Ogawa, M. 1971, *JChPh*, **54**, 2550
- Ogawa, S., & Ogawa, M. 1975, *CaJPh*, **53**, 1845
- Piccialli, A., Montmessin, F., Belyaev, D., et al. 2015, *P&SS*, **113**, 321
- Roth, L., Ivchenko, N., Gladstone, G. R., et al. 2021, *NatAs*, **5**, 1043
- Roth, L., Saur, J., Retherford, K. D., Strobel, D. F., & Spencer, J. R. 2011, *Icar*, **214**, 495
- Roth, L., Saur, J., Retherford, K. D., et al. 2016, *JGRA*, **121**, 2143
- Sandel, B. R., Gröller, H., Yelle, R. V., et al. 2015, *Icar*, **252**, 154
- Stern, S. A., Slater, D. C., Scherrer, J., et al. 2007, *SSRv*, **128**, 507
- Stern, S. A., Slater, D. C., Scherrer, J., et al. 2008, *SSRv*, **140**, 155
- Strobel, D. F., Summers, M. E., Herbert, F., & Sandel, B. R. 1990, *GeoRL*, **17**, 1729
- Velez, M. A., Retherford, K. D., Hue, V., et al. 2022, *Proc. SPIE*, **12181**, 33
- Watanabe, K., & Marmo, F. F. 1956, *JChPh*, **25**, 965
- Wenger, M., Ochsenbein, F., Egret, D., et al. 2000, *A&AS*, **143**, 9
- Young, L. A., Kammer, J. A., Steffl, A. J., et al. 2018, *Icar*, **300**, 174